



Dalton  
Transactions

**A Series of  $\text{Rb}_4\text{Ln}_2(\text{P}_2\text{S}_6)(\text{PS}_4)_2$  (Ln = La, Ce, Pr, Nd, Sm, Gd) Rare Earth Thiophosphates with Two Distinct Thiophosphate Units  $[\text{PVS}_4]^{3-}$  and  $[\text{PIV}_2\text{S}_6]^{4-}$**

Journal:	<i>Dalton Transactions</i>
Manuscript ID	DT-ART-10-2020-003718.R1
Article Type:	Paper
Date Submitted by the Author:	04-Jan-2021
Complete List of Authors:	Kutahyali Aslani, Ceren; University of South Carolina, Breton, Logan; University of South Carolina Klepov, Vladislav; University of South Carolina, Department of Chemistry and Biochemistry Zur Loye, Hans-Conrad; University of South Carolina, Department of Chemistry and Biochemistry

SCHOLARONE™  
Manuscripts

**A Series of  $\text{Rb}_4\text{Ln}_2(\text{P}_2\text{S}_6)(\text{PS}_4)_2$  (Ln = La, Ce, Pr, Nd, Sm, Gd) Rare Earth Thiophosphates with Two Distinct Thiophosphate Units  $[\text{P}^{\text{V}}\text{S}_4]^{3-}$  and  $[\text{P}^{\text{IV}}_2\text{S}_6]^{4-}$**

*Ceren Kutahyali Aslani, Logan S. Breton, Vladislav V. Klepov, and Hans-Conrad zur Loye\**

Department of Chemistry and Biochemistry, University of South Carolina, Columbia, SC 29208

## Abstract

A series of rubidium rare earth thiophosphates with the formula  $\text{Rb}_4\text{Ln}_2(\text{P}_2\text{S}_6)(\text{PS}_4)_2$  ( $\text{Ln} = \text{La, Ce, Pr, Nd, Sm, and Gd}$ ) was synthesized using the high temperature molten flux crystal growth method utilizing a RbBr flux. Single crystals of all title compounds, as well as phase pure powders of the La-, Ce-, and Sm-containing compositions, were obtained. Single crystals of the title compounds were characterized by single crystal and powder X-ray diffraction for structure and phase identification.  $\text{Rb}_4\text{Ln}_2(\text{P}_2\text{S}_6)(\text{PS}_4)_2$  crystallizes in the monoclinic crystal system adopting the  $P2_1/n$  space group for the large rare earths ( $\text{Ln} = \text{La, Ce, Pr}$ ) and the  $C2/c$  space group for the smaller rare earths ( $\text{Ln} = \text{Nd, Sm, Gd}$ ). This  $\text{Rb}_4\text{Ln}_2(\text{P}_2\text{S}_6)(\text{PS}_4)_2$  series is a rare example of thiophosphates containing both tetrahedral  $[\text{P}^{\text{V}}\text{S}_4]^{3-}$  and dimeric  $[\text{P}^{\text{IV}}_2\text{S}_6]^{4-}$  thiophosphate units that, in this structural family, link corrugated rare earth sulfide chains into sheets. The band gaps of the materials were determined from UV-Vis data and the fluorescence spectrum of  $\text{Rb}_4\text{Ce}_2(\text{P}_2\text{S}_6)(\text{PS}_4)_2$  was collected. Optical band gaps were estimated to be 2.9, and 2.4 for the Nd, and Sm analogues respectively.

## Introduction

Rare earth and transition metal sulfides have been of interest for decades for their numerous physical properties where, at different times, the specific materials on which research focused depended typically on a specific application of interest at that time. Thus, recently thiophosphates have attracted much interest when it was discovered that select thiophosphate compositions exhibit very high ion conductivity,<sup>1</sup> which has quickly generated general interest in developing synthetic approaches that can lead to single crystals of the desired thiophosphate compositions. Our group has explored the crystal growth of a number of thiophosphate compositions, including rare earth<sup>2,3</sup> and uranyl thiophosphates,<sup>4</sup> to investigate their unique structural features and we have demonstrated that in many cases the topologies are quite modular allowing many of their structures to be described as being assembled from simple building blocks.

To expand the number of known thiophosphates, for structural rather than ionic conductivity reasons, we have explored the use of different fluxes to crystallize unique compositions with interesting structural features. The structural variety of the thiophosphate compounds can be attributed to the different thiophosphate building blocks that can be used to create complex structures where, specifically, building blocks such as ortho-thiophosphate  $P^V S_4^{3-}$ ,<sup>5-12</sup> thiopyrophosphate  $P^V_2 S_7^{4-}$ ,<sup>13-15</sup> hexathiometadiphosphate  $P^V_2 S_6^{2-}$ ,<sup>15,19</sup> as well as the reduced hexathiohypophosphate,  $P^{IV}_2 S_6^{4-}$ <sup>2,13,17-19</sup> have been observed in a large number of thiophosphate phases. However, in the majority of the known rare earth thiophosphates, only one thiophosphate unit is typically present in any given structure<sup>3,4,12,14,18,20,21</sup> and there are only a few rare earth thiophosphate structures that simultaneously incorporate multiple thiophosphate units<sup>4,13,19</sup>. As the combination of multiple thiophosphate units could increase the structural diversity via more variability in the connection of polyhedra within the structure, we have focused on the flux crystal growth<sup>22,23</sup> of rare earth thiophosphates with an emphasis on exploring different fluxes in order to establish their suitability for growing complex thiophosphate structures.

Based on the previous successful work on the synthesis of lanthanide thiophosphates, e.g.  $K_3 Ce P_2 S_8$ ,<sup>24</sup> our group recently published on several families of alkali metal rare earth thiophosphates, including chain containing  $Cs_2 Na Ln (PS_4)_2$  ( $Ln = La-Nd, Sm, \text{ and } Gd-Ho$ ),<sup>12</sup>

layer containing thiohypophosphates  $\text{NaLnP}_2\text{S}_6$  ( $\text{Ln} = \text{La, Ce, Pr}$ )<sup>2</sup> and thiopyrophosphates  $\text{CsLnP}_2\text{S}_7$  ( $\text{Ln} = \text{Pr, Nd, Sm, Gd, Tb, Dy, Ho, Er, Yb, Y}$ )<sup>2</sup>, as well as several other mixed alkali metal thiophosphates  $\text{Cs}_3\text{La}_5(\text{PS}_4)_6$ ,  $\text{Cs}_3\text{Ce}_5(\text{PS}_4)_6$ ,  $\text{Cs}_3\text{Sm}_3(\text{PS}_4)_4$ , and  $\text{Cs}_3\text{Dy}_3(\text{PS}_4)_4$ <sup>12</sup>. In all of these structures, the thiophosphate groups are attached to the rare earth polyhedra and often decorate rare earth sulfide chains. The presence of a linking group is generally needed to convert chains into layers, as will be described for the title compounds herein. We had focused on cesium containing phases as the reactive CsI flux proved effective for growing crystals of cesium containing thiophosphates. There are relatively few examples of rubidium containing rare earth thiophosphates compared to those containing potassium and cesium. The first rubidium rare earth thiophosphates were synthesized by Komm and Schleid<sup>20</sup> with the formulas  $\text{Rb}_3\text{Pr}_3(\text{PS}_4)_4$  and  $\text{Rb}_3\text{Er}_3(\text{PS}_4)_4$ . Subsequently, only a handful of rubidium rare earth thiophosphates have been synthesized, including  $\text{RbLaP}_2\text{S}_6$ ,<sup>18</sup>  $\text{Rb}_3\text{Sm}(\text{PS}_4)_2$ ,<sup>10</sup> and  $\text{Rb}_3\text{Gd}(\text{PS}_4)_2$ .<sup>3</sup> Changing the flux from CsI to RbBr, and expecting the RbBr flux to be reactive, we targeted new rubidium containing rare earth thiophosphates.<sup>12</sup>

Herein we report the successful flux synthesis and crystal structures of a new series of rubidium rare earth thiophosphates with the formula,  $\text{Rb}_4\text{Ln}_2(\text{P}_2\text{S}_6)(\text{PS}_4)_2$  ( $\text{Ln} = \text{La, Ce, Pr, Nd, Sm, and Gd}$ ), which contain both the  $[\text{P}^{\text{V}}\text{S}_4]^{3-}$  and  $[\text{P}^{\text{IV}}_2\text{S}_6]^{4-}$  thiophosphate units within their crystal structures. Phase pure samples of the  $\text{Ln} = \text{Ce, Nd and Sm}$  were obtained and their optical and magnetic properties were measured. Experiments with Er, Tb, Dy, Ho, Tm, Yb were not successful and did not result in any crystals.

## EXPERIMENTAL

### Reagents

$\text{P}_2\text{S}_5$  (99%, Sigma-Aldrich),  $\text{Na}_2\text{S}$  (Alfa Aesar), N,N-dimethylformamide (DMF, Sigma-Aldrich, ACS grade)  $\text{La}_2\text{S}_3$  (STREM Chemicals Inc., 99.9%),  $\text{CeO}_2$  (Alfa Aesar, 99.99%),  $\text{Pr}_6\text{O}_{11}$  (Alfa Aesar, 99.99%),  $\text{Nd}_2\text{O}_3$  (Alfa Aesar, 99.99%),  $\text{Sm}_2\text{O}_3$  (Alfa Aesar, 99.99%),  $\text{Gd}_2\text{O}_3$  (Alfa Aesar, 99.99%),  $\text{Er}_2\text{O}_3$  (Alfa Aesar, 99.99%),  $\text{Tb}_4\text{O}_7$  (Alfa Aesar, 99.9%),  $\text{Tm}_2\text{O}_3$  (Alfa Aesar, 99.99%),  $\text{Dy}_2\text{O}_3$  (Alfa Aesar, 99.9%),  $\text{Ho}_2\text{O}_3$  (Alfa Aesar, 99.99%),  $\text{Yb}_2\text{O}_3$  (Alfa Aesar, 99.99%) were all used as received.  $\text{P}_2\text{S}_5$  and  $\text{Na}_2\text{S}$  were stored and handled in a nitrogen glovebag. Rare earth sulfides, excluding  $\text{La}_2\text{S}_3$ , were prepared according to the procedure described in the literature.<sup>2,25</sup>

## Synthesis

$\text{Rb}_4\text{Ln}_2(\text{P}_2\text{S}_6)(\text{PS}_4)_2$  ( $\text{Ln} = \text{La}, \text{Ce}, \text{Pr}, \text{Nd}, \text{Sm}, \text{and Gd}$ ) were all obtained under identical synthetic conditions.  $\text{Ln}_2\text{S}_3$  (0.1656 mmol),  $\text{Na}_2\text{S}$  (0.662 mmol), and  $\text{P}_2\text{S}_5$  (0.662 mmol), in a 1:4:4 molar ratio, were used along with 1.0 g of RbBr flux. The reagents were loaded into a fused silica tube (~120 mm long, 10 and 12 mm inner and outer diameters, respectively) inside a nitrogen glove bag, flame-sealed under vacuum and placed in a programmable furnace. The furnace was ramped up to 800 °C in 1 h, held at that temperature for 12 h, followed by slow cooling at 10°C/h rate to 460°C, and subsequently cooled to room temperature by switching off the furnace. The flux was removed by dissolving it in ~50 mL of DMF aided by sonication, and the resulting products were isolated by vacuum-filtration.

## Single Crystal X-ray Diffraction

Single-crystal X-ray diffraction data were collected at 300(2) K on a Bruker D8 QUEST diffractometer equipped with an Incoatec  $\text{I}\mu\text{S}$  3.0 microfocus radiation source ( $\text{MoK}\alpha$ ,  $\lambda = 0.71073 \text{ \AA}$ ) and a PHOTON II area detector. The crystals were mounted on a microloop using immersion oil. The raw data reduction and absorption corrections were performed using SAINT and SADABS programs<sup>26,27</sup>. Initial structure solutions were obtained with SHELXS-2017 using direct methods and Olex2 GUI.<sup>28</sup> Full-matrix least-squares refinements against  $F^2$  were performed with SHELXL software.<sup>29</sup> The crystallographic data and results of the diffraction experiments are summarized in Table 1 and Tables S1-S6.

Table 1. Crystallographic Data for  $\text{Rb}_4\text{Ln}_2(\text{P}_2\text{S}_6)(\text{PS}_4)_2$  ( $\text{Ln}=\text{La}, \text{Ce}, \text{Pr}, \text{Nd}, \text{Sm}, \text{and Gd}$ )

Chemical formula	$\text{Rb}_4\text{La}_2(\text{P}_2\text{S}_6)(\text{PS}_4)_2$	$\text{Rb}_4\text{Ce}_2(\text{P}_2\text{S}_6)(\text{PS}_4)_2$	$\text{Rb}_4\text{Pr}_2(\text{P}_2\text{S}_6)(\text{PS}_4)_2$	$\text{Rb}_4\text{Nd}_2(\text{P}_2\text{S}_6)(\text{PS}_4)_2$	$\text{Rb}_4\text{Sm}_2(\text{P}_2\text{S}_6)(\text{PS}_4)_2$	$\text{Rb}_4\text{Gd}_2(\text{P}_2\text{S}_6)(\text{PS}_4)_2$
Formula weight	1192.42	1194.84	1196.42	1203.08	1215.30	1229.10
Crystal system	Monoclinic					
Space group, $Z$	$P2_1/n$			$C2/c$		
$a$ , Å	9.4993(2)	9.4771(2)	9.4631(2)	22.9712(5)	22.8828(5)	22.8259(4)
$b$ , Å	6.84630(10)	6.8346(2)	6.83090(10)	6.82480(10)	6.80720(10)	6.79290(10)
$c$ , Å	19.8176(4)	19.7215(5)	19.6643(4)	18.8874(4)	18.8375(4)	18.7916(3)
$\beta$ , deg.	98.1714(7)	98.1350(10)	98.0659(7)	122.0390(7)	121.9120(10)	121.7523(6)
$V$ , Å <sup>3</sup>	1275.75(4)	1264.55(6)	1258.55(4)	2510.04(9)	2490.79(9)	2477.62(7)
$\rho_{\text{calcd}}$ , g/cm <sup>3</sup>	3.11	3.14	3.16	3.18	3.24	3.30
Radiation ( $\lambda$ , Å)	MoK $\alpha$ (0.71073)					
$\mu$ , mm <sup>-1</sup>	12.27	12.60	12.92	13.21	13.86	14.54
$T$ , K	302 K	301 K	302(2)	300(2)	303(2)	302(2)
Crystal dim., mm <sup>3</sup>	0.06×0.06×0.04	0.07×0.06×0.01	0.06×0.06×0.02	0.11×0.08×0.04	0.04×0.04×0.01	0.06×0.05×0.04
$2\theta$ range, deg.	2.532- 29.998	2.086-30.00	2.541-29.994	3.163- 27.499	2.547- 29.999	2.549- 29.998
Reflections collected	27582	45198	72275	48114	50286	41258
Data/parameters/restraints	3727/109/0	3706/109/0	3683/109/0	2859/109/0	3643/109/0	3616/109/0
$R_{\text{int}}$	0.0354	0.0451	0.0444	0.0298	0.0465	0.0311
Goodness of fit	1.025	1.105	1.060	1.045	1.103	1.101
$R_1(I > 2\sigma(I))$	0.0204	0.0304	0.0161	0.0211	0.0227	0.0158
$wR_2(\text{all data})$	0.0440	0.0606	0.0370	0.0558	0.0481	0.0326

### **Powder X-ray Diffraction**

Powder X-ray diffraction (PXRD) data for phase purity confirmation were collected on polycrystalline samples ground from single crystals. Data were collected on a Bruker D2 PHASER diffractometer using Cu K $\alpha$  radiation over a  $2\theta$  range 10–65° with a step size of 0.02°.

### **Energy-Dispersive Spectroscopy (EDS)**

EDS was performed on single crystal products using a Tescan Vega-3 SEM equipped with a Thermo EDS attachment. The SEM was operated in low-vacuum mode. Crystals were mounted on an SEM stub with carbon tape and analyzed using a 20 kV accelerating voltage and an 80 s accumulation time. The results of EDS confirm the presence of elements found by single-crystal X-ray diffraction.

### **Optical Properties**

UV–vis spectra of Rb<sub>4</sub>Nd<sub>2</sub>(P<sub>2</sub>S<sub>6</sub>)(PS<sub>4</sub>)<sub>2</sub> and Rb<sub>4</sub>Sm<sub>2</sub>(P<sub>2</sub>S<sub>6</sub>)(PS<sub>4</sub>)<sub>2</sub> were recorded using a Perkin Elmer Lambda 35 UV/Visible scanning spectrophotometer used in the diffuse reflectance mode and equipped with an integrating sphere. Diffuse reflectance spectra were recorded in the 200–900 nm range. Reflectance data were converted to absorbance using the Kubelka–Munk function.

Fluorescence measurements were collected on a PerkinElmer LS 55 spectrometer. Excitation spectra were collected at an emission wavelength of 539 nm, and emission spectra were collected at an excitation wavelength of 378 nm

### **Magnetism**

Magnetic property measurements for Rb<sub>4</sub>Ce<sub>2</sub>(P<sub>2</sub>S<sub>6</sub>)(PS<sub>4</sub>)<sub>2</sub>, Rb<sub>4</sub>Nd<sub>2</sub>(P<sub>2</sub>S<sub>6</sub>)(PS<sub>4</sub>)<sub>2</sub> and Rb<sub>4</sub>Sm<sub>2</sub>(P<sub>2</sub>S<sub>6</sub>)(PS<sub>4</sub>)<sub>2</sub> were performed using a Quantum Design MPMS 3 SQUID magnetometer. Zero-field-cooled (ZFC) magnetic susceptibility data were collected from 2 to 300 K in an applied field of 0.1 T. The raw data were corrected for radial offset and sample shape effects according to the method described in the literature.<sup>30</sup>

## RESULTS AND DISCUSSION

### Synthesis

The use of CsI as a flux to prepare cesium containing thiophosphates had been extremely successful yielding, among others, the  $\text{Cs}_2\text{NaLn}(\text{PS}_4)_2$  ( $\text{Ln} = \text{La, Ce, Pr, Gd, Tb, Dy, and Ho}$ ) family of thiophosphates.<sup>12</sup> To expand on these results and to explore the effect of the alkali metal cation size, we targeted the crystal growth of rubidium containing rare earth thiophosphates. Switching from CsI to RbBr as the flux, but otherwise utilizing the same starting materials and reagent ratios, we identified reaction conditions under which crystals formed. This resulted in single crystals of a new series of rubidium rare earth thiophosphates with the chemical formula  $\text{Rb}_4\text{Ln}_2(\text{P}_2\text{S}_6)(\text{PS}_4)_2$  ( $\text{Ln} = \text{La, Ce, Pr, Nd, Sm, and Gd}$ ). In addition to crystals, several reactions also yielded phase pure powders, specifically in the case of  $\text{Ln} = \text{La, Ce, and Sm}$ . Attempts to expand this family to the smaller rare earths ( $\text{Ln} = \text{Tb, Dy, Er, Tm and Yb}$ ) using the same reaction conditions did not result in a single crystalline product. It is likely that crystals containing these rare earths can be prepared, however, perhaps not with the same crystal structure due to the decrease in the lanthanide size.

The  $\text{Rb}_4\text{Ln}_2(\text{P}_2\text{S}_6)(\text{PS}_4)_2$  structure contains, simultaneously, the  $\text{P}^{\text{V}}\text{S}_4^{3-}$  and the  $\text{P}^{\text{IV}}_2\text{S}_6^{4-}$  thiophosphate motifs. As  $\text{P}^{\text{V}}_2\text{S}_5$  was used as a starting reagent, the creation of the  $\text{P}^{\text{IV}}_2\text{S}_6^{4-}$  motif requires an *in situ* reduction of the phosphorus from +5 to +4 during the reaction, a phenomena observed previously.<sup>2</sup> While the identity of the reducing agent has yet to be explicitly determined, one can surmise that reduced phosphorus incorporation into the final product occurred because there is a dynamic equilibrium between different types of phosphorus units, containing phosphorous in different oxidation states, in the flux environment at the high temperatures used in the synthesis. Unlike reactions utilizing the CsI flux, which resulted in iodine sublimation to the top of the reaction vessels that could potentially act as a reducing agent, it is less likely that the bromide anions play the role of a reducing agent in these reactions. This suggests that the reduction of phosphorus in these reactions takes place no matter the identity of the halide used in the flux. All compositions reported herein are stable for at least one year when stored in closed plastic vials.

## Crystal Structure

The  $\text{Rb}_4\text{Ln}_2(\text{P}_2\text{S}_6)(\text{PS}_4)_2$  series crystallizes in the monoclinic crystal system in either the  $P2_1/n$  space group for the larger lanthanides ( $\text{Ln} = \text{La}, \text{Ce}, \text{Pr}$ ) or in the  $C2/c$  space group for the smaller lanthanides ( $\text{Ln} = \text{Nd}, \text{Sm}, \text{Gd}$ ). The crystal structures of  $\text{Rb}_4\text{Ln}_2(\text{P}_2\text{S}_6)(\text{PS}_4)_2$  (Figure 1) consist of lanthanide thiophosphate layers separated by Rb cations (Figure 1g). The topology of the lanthanide thiophosphate layers is the same for the two space groups (Figure 1f) and to the previously reported  $\text{K}_4\text{Ln}_2(\text{P}_2\text{S}_6)(\text{PS}_4)_2$  ( $\text{Ln} = \text{La}, \text{Nd}, \text{Sm}$ ).<sup>8,13,17</sup> In both structures, the lanthanide cations are located in 8-fold bicapped trigonal prismatic coordination environments, where the polyhedra connect to adjacent lanthanides via corner sharing to form corrugated chains (Fig. 1c). The lanthanide polyhedra within the chains are further linked to each other by  $\text{PS}_4$  tetrahedra that decorate the sides of the lanthanide chains via edge sharing with two neighboring lanthanide polyhedra and corner sharing with a third (Fig. 1d). The chains are linked to each other through  $\text{P}_2\text{S}_6$  groups that face share with the lanthanide polyhedra creating the  $[\text{Ln}_2(\text{P}_2\text{S}_6)(\text{PS}_4)_2]^{4-}$  layers (Fig 1e). The lanthanide polyhedra have Ln-S bond length ranging from 2.8456(8) to 3.2829(9) Å, agreeing well with Ln-S bond lengths previously reported in the literature.<sup>2,19</sup> Rb-S bond lengths range from 3.3218(6) to 3.8762(7) Å. The P–P and P–S bond distances fall within the ranges of 2.1931(16)–2.1980(2) and 1.9909(7)–2.0568(9) Å, respectively. As described previously, one can denote common coordination types for the thiophosphate anions.<sup>4</sup> All  $\text{PS}_4$  thiophosphate units in the structure can be described as having a  $Q^{120}$  coordination type, the  $Q$  denoting a tetradentate coordination mode and the 1, 2, and 0 denoting the number of corner, edge, and face-shares, respectively. The  $\text{P}_2\text{S}_6$  thiophosphate unit can be described as having a  $\text{H}^{002}$  coordination type. Although the crystals of  $\text{Rb}_4\text{Ln}_2(\text{P}_2\text{S}_6)(\text{PS}_4)_2$  change their symmetry from  $P2_1/n$  to  $C2/c$  when  $\text{Ln} = \text{La–Pr}$ , and  $\text{Nd–Gd}$ , respectively, the atomic arrangement in both symmetries is almost identical (Figure 1g and h) with only small rotations of thiophosphate units. As illustrated for the Tl analogs, both compounds are related to the same supergroup structure with  $C2/m$  symmetry.<sup>31,32</sup>

In our previous studies<sup>2,12</sup> we observed that when moving across the lanthanide series, the coordination number of the lanthanide cations tends to decrease from 9 to 8, as a result of the lanthanide contraction. Due to this contraction, typically, we observe a change in the crystal structure at some point across the series. Klepov et al.<sup>12</sup> discussed this transition in detail and

characterize the change in coordination number from 9 to 8 along the lanthanide series. In our case, for this system, the late lanthanides (Tb, Dy, Ho, Er, Tm, Yb) did not result in any crystals.

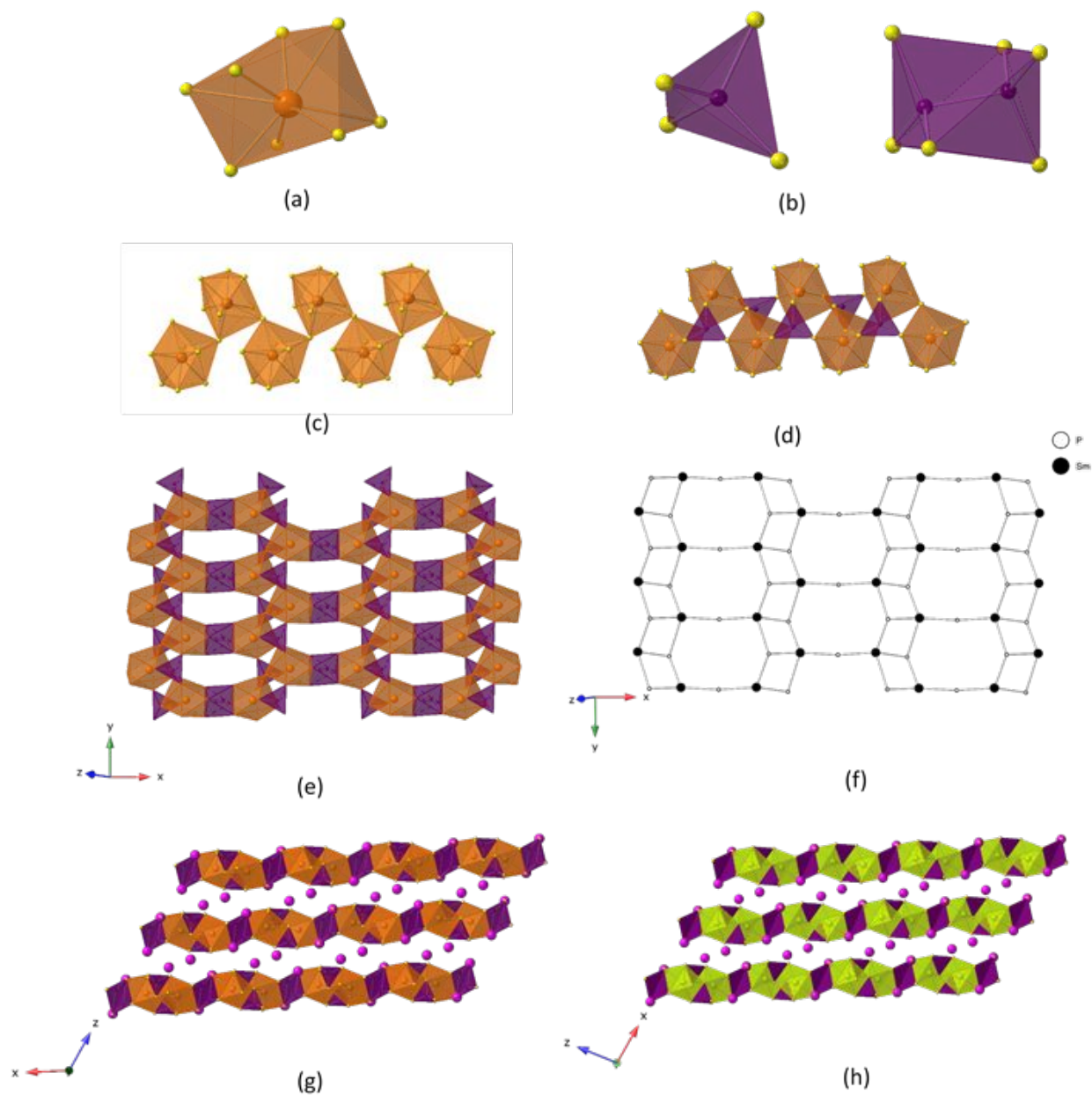


Figure 1. (a) SmS<sub>8</sub> coordination polyhedra, (b) (PS<sub>4</sub>)<sup>3-</sup> and (P<sub>2</sub>S<sub>6</sub>)<sup>4-</sup> units, (c) and (d) their connection to chains running along the y axis (e) Sm<sub>2</sub>(P<sub>2</sub>S<sub>6</sub>)(PS<sub>4</sub>)<sub>2</sub> layers (f) their topology (g) structure of Rb<sub>4</sub>Sm<sub>2</sub>(P<sub>2</sub>S<sub>6</sub>)(PS<sub>4</sub>)<sub>2</sub> and (h) structure of Rb<sub>4</sub>Ce<sub>2</sub>(P<sub>2</sub>S<sub>6</sub>)(PS<sub>4</sub>)<sub>2</sub>. Samarium, cerium, phosphorus, and rubidium atoms are colored orange, green, purple and pink, respectively.

## Optical Properties

Diffuse reflectance UV/Vis spectra were collected for ground powders of  $\text{Rb}_4\text{Nd}_2(\text{P}_2\text{S}_6)(\text{PS}_4)_2$  (blue) and  $\text{Rb}_4\text{Sm}_2(\text{P}_2\text{S}_6)(\text{PS}_4)_2$  (yellow-green). The f-f transitions characteristic of the localized 4f orbitals of the lanthanides were resolved.<sup>33</sup> Converting the diffuse reflectance spectra (Fig 2) to optical energy plots shows the sharp absorption edges characteristic of semiconducting materials. Optical band gaps were estimated to be 2.9, and 2.4 for the Nd, and Sm analogues respectively. The estimated band gaps agree well with the observed colors of the compounds.

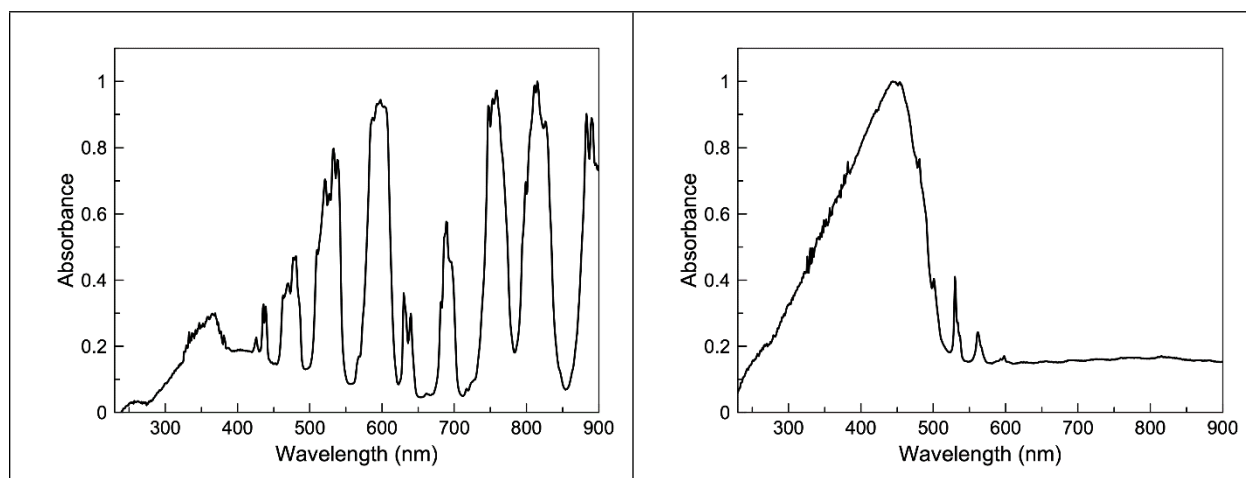


Figure 2. The UV-vis spectrum of (left)  $\text{Rb}_4\text{Nd}_2(\text{P}_2\text{S}_6)(\text{PS}_4)_2$  and (right)  $\text{Rb}_4\text{Sm}_2(\text{P}_2\text{S}_6)(\text{PS}_4)_2$

All crystals were checked for fluorescence under UV light excitation and only  $\text{Rb}_4\text{Ce}_2(\text{P}_2\text{S}_6)(\text{PS}_4)_2$  showed strong green-yellow fluorescence. Fluorescence measurements were performed on  $\text{Rb}_4\text{Ce}_2(\text{P}_2\text{S}_6)(\text{PS}_4)_2$  using an excitation wavelength of 378 nm with a maximum emission peak at 539 nm (Figure 3).

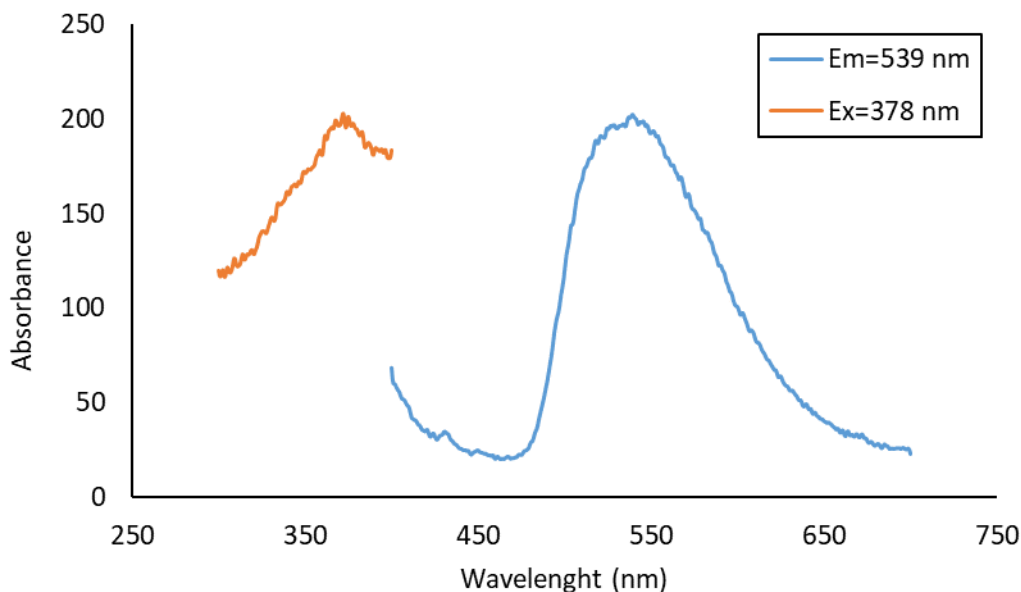
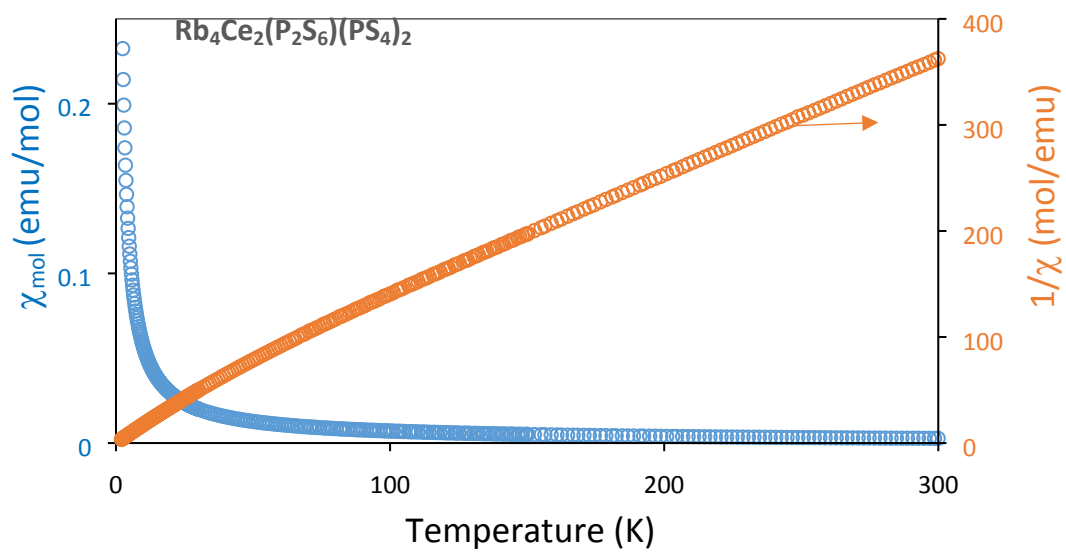
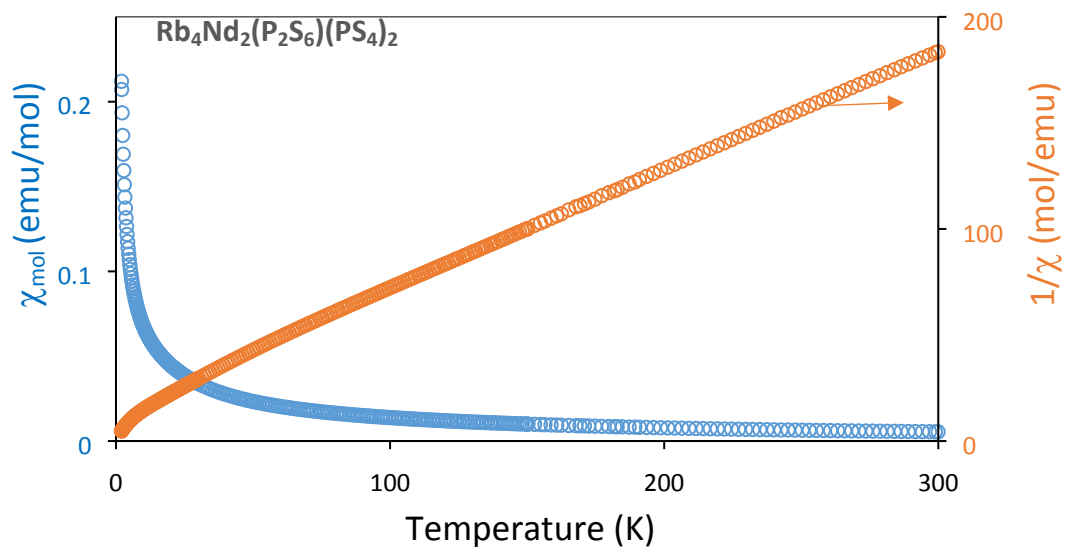


Figure 3. Fluorescence excitation and emission spectra of  $\text{Rb}_4\text{Ce}_2(\text{P}_2\text{S}_6)(\text{PS}_4)_2$ .

### Magnetic Properties

Magnetic susceptibility data over the temperature range of 2-300K were collected for  $\text{Rb}_4\text{Ce}_2(\text{P}_2\text{S}_6)(\text{PS}_4)_2$ ,  $\text{Rb}_4\text{Nd}_2(\text{P}_2\text{S}_6)(\text{PS}_4)_2$ , and  $\text{Rb}_4\text{Sm}_2(\text{P}_2\text{S}_6)(\text{PS}_4)_2$  (Figure 4). The Ln = Ce and Nd analogues follow the Curie-Weiss law and effective magnetic moments were obtained from fits of the susceptibility data to the Curie-Weiss law. The effective moments of  $2.66 \mu_{\text{B}}$  and  $3.77 \mu_{\text{B}}$  for Ln – Ce and Nd, respectively, closely match the calculated values of  $2.54 \mu_{\text{B}}$  and  $3.63 \mu_{\text{B}}$ . The Sm compound exhibits Van Vleck paramagnetism due to mixing of ground and excited states.<sup>34</sup> The magnetic moment of  $1.57 \mu_{\text{B}}$  was determined from the molar susceptibility versus temperature plots at 300 K. This moment compares well to the reported moments of 1.4-1.7.<sup>35</sup> None of the three compositions exhibited any indication of long range magnetic order, which is not unexpected due to rather long Ln-Ln separations observed for the three compositions. The Ln-Ln distances range from 5.421, 5.447, 5.387 Å for Nd, Ce and Sm, respectively, all significantly larger than any distance for which one would expect magnetic interactions for highly localized 4f orbitals.



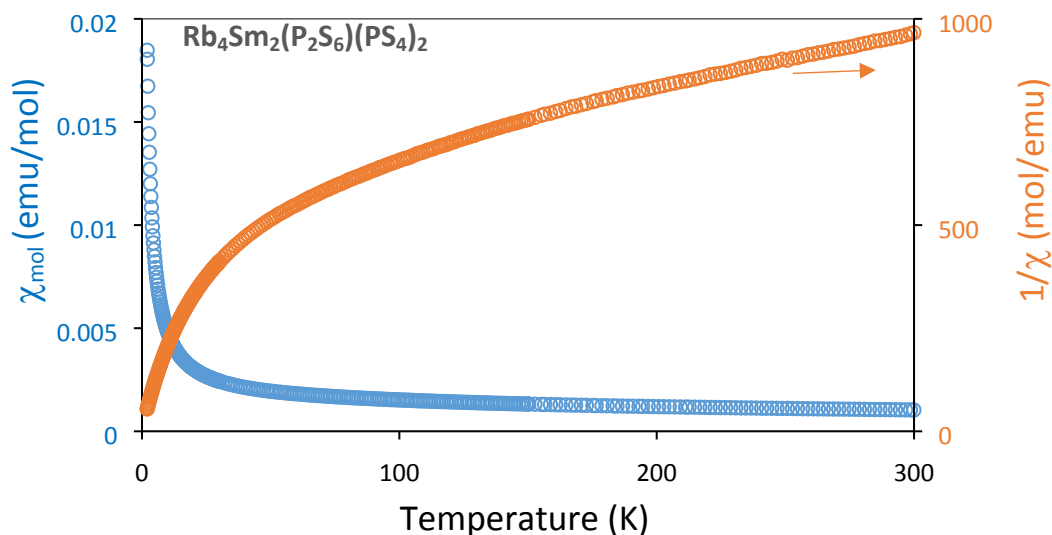


Figure 4. Plots of the temperature dependence of the magnetic susceptibilities and inverse susceptibilities for  $\text{Rb}_4\text{Nd}_2(\text{P}_2\text{S}_6)(\text{PS}_4)_2$ ,  $\text{Rb}_4\text{Ce}_2(\text{P}_2\text{S}_6)(\text{PS}_4)_2$ , and  $\text{Rb}_4\text{Sm}_2(\text{P}_2\text{S}_6)(\text{PS}_4)_2$ .

## CONCLUSION

A series of new rare earth thiophosphates,  $\text{Rb}_4\text{Ln}_2(\text{P}_2\text{S}_6)(\text{PS}_4)_2$  ( $\text{Ln}=\text{La}, \text{Ce}, \text{Pr}, \text{Nd}, \text{Sm}, \text{Gd}$ ), were prepared via high-temperature flux crystal growth in evacuated silica tubes using a RbBr flux. The  $\text{Rb}_4\text{Ln}_2(\text{P}_2\text{S}_6)(\text{PS}_4)_2$  structure contains two thiophosphate motifs,  $\text{P}^{\text{V}}\text{S}_4^{3-}$  and  $\text{P}^{\text{IV}}_2\text{S}_6^{4-}$ , within the crystal structure. The compounds crystallize in the monoclinic crystal system with space groups  $P2_1/n$  for the larger lanthanides ( $\text{Ln} = \text{La}, \text{Ce}, \text{Pr}$ ) and in the space group  $C2/c$  for the smaller lanthanides ( $\text{Ln} = \text{Nd}, \text{Sm}, \text{Gd}$ ). The topologies of these structures are quite modular enabling their description as being assembled from simple building blocks. The magnetic properties of  $\text{Rb}_4\text{Ln}_2(\text{P}_2\text{S}_6)(\text{PS}_4)_2$  ( $\text{Ln}=\text{Ce}, \text{Nd}$  and  $\text{Sm}$ ) were characterized by magnetic susceptibility measurements. The magnetic moments agree with the calculated moments and no indication of long-range magnetic order was observed. UV/Vis measurements allowed the typical f-f transitions characteristic to the 4f orbitals of the lanthanides to be resolved. Fluorescence measurements performed on  $\text{Rb}_4\text{Ce}_2(\text{P}_2\text{S}_6)(\text{PS}_4)_2$  show strong yellow-green luminesces using an excitation wavelength of 378 nm with a maximum emission intensity at 539 nm.

**Supporting information**

PXRD patterns (Figures S1-S3), EDS results (Figure S4-10 and Table S7), Effective Magnetic Moments and Weiss Constants (Table S8) PDF). CSD 2040663–2040668 contain the supplementary crystallographic data for this paper. The data can be obtained free of charge from The Cambridge Crystallographic Data Centre via [www.ccdc.cam.ac.uk/structures](http://www.ccdc.cam.ac.uk/structures).

**Acknowledgment**

Research supported by the US Department of Energy, Office of Basic Energy Sciences, Division of Materials Sciences and Engineering under award DE-SC0018739.

## REFERENCES

1. S. Seidel, W.G. Zeier, R. Pöttgen, The polymorphs of the Na<sup>+</sup> ion conductor Na<sub>3</sub>PS<sub>4</sub> viewed from the perspective of a group-subgroup scheme. *Z. Kristallogr. Cryst. Mater.* 2020;235:1-6.
2. V.V. Klepov, L.S. Breton, K.A. Pace, V. Kocevski, T.M. Besmann, H.C. zur Loye, Size-Driven Stability of Lanthanide Thiophosphates Grown from an Iodide Flux. *Inorg Chem.* 2019;58(9):6565-6573. doi:10.1021/acs.inorgchem.9b00806
3. M. Usman, M.D. Smith, V.V. Klepov, H.C. zur Loye, One-Dimensional Quaternary and Pentanary Alkali Rare Earth Thiophosphates Obtained via Alkali Halide Flux Crystal Growth. *Cryst Growth Des.* 2019;19(10):5648-5657. doi:10.1021/acs.cgd.9b00637
4. V.V. Klepov, H.C. zur Loye, Complex Topologies from Simple Building Blocks: Uranium(IV) Thiophosphates. *Inorg Chem.* 2018;57(17):11175-11183. doi:10.1021/acs.inorgchem.8b01733
5. T. Komm, T. Schleid, Drei alkalimetall-erbium-thiophosphate: Von der schichtstruktur bei KEr[P<sub>2</sub>S<sub>7</sub>] zur dreidimensionalen vernetzung in NaEr[P<sub>2</sub>S<sub>6</sub>] und Cs<sub>3</sub>Er<sub>5</sub>[PS<sub>4</sub>]<sub>6</sub>. *Zeitschrift für Anorg und Allg Chemie.* 2006;632(1):42-48. doi:10.1002/zaac.200500332
6. T. Komm, T. Schleid, Li<sub>9</sub>Nd<sub>2</sub>[PS<sub>4</sub>]<sub>5</sub>: A new lithium lanthanoid(III) thiophosphate(V). *J Alloys Compd.* 2006;418(1-2):106-110. doi:10.1016/j.jallcom.2005.09.089
7. C. Müller, S. Jörgens, A. Mewis, Neue Thiophosphate: Die Verbindungen Li<sub>6</sub>Ln<sub>3</sub>(PS<sub>4</sub>)<sub>5</sub> (Ln: Y, Gd, Dy, Yb, Lu) und Ag<sub>3</sub>Y(PS<sub>4</sub>)<sub>2</sub>. *Zeitschrift für Anorg und Allg Chemie.* 2007;633(10):1633-1638. doi:10.1002/zaac.200700065
8. V. Manríquez, A. Galdámez, D. Guzmán-Águila, New quaternary alkali metal, rare earth (3+) thiophosphate, K<sub>2</sub>SmP<sub>2</sub>S<sub>7</sub> with both [P<sub>2</sub>S<sub>6</sub>]<sup>4-</sup> and [PS<sub>4</sub>]<sup>3-</sup> anions. *Mater Res Bull.* 2008;43(8-9):2469-2475. doi:10.1016/j.materresbull.2007.07.028
9. Y. Klawitter, W. Bensch, C. Wickleder, Synthesis, crystal structure, and vibrational and optical spectroscopy of the first quaternary alkaline-earth rare earth thiophosphates Ba<sub>3</sub>Ln<sub>2</sub>[P<sub>4</sub>S<sub>16</sub>] (Ln = Gd-Er). *Chem Mater.* 2006;18(1):187-197. doi:10.1021/cm051860n
10. S. Milot, Y. Wu, C. Näther, W. Bensch, K.O. Klepp, Two new quaternary thiophosphates with pseudo one-dimensional structures: Syntheses and crystal structures of Cs<sub>3</sub>Sm[PS<sub>4</sub>]<sub>2</sub> and Rb<sub>3</sub>Sm[PS<sub>4</sub>]<sub>2</sub>. *Zeitschrift für Anorg und Allg Chemie.* 2008;634(9):1575-1580. doi:10.1002/zaac.200800154
11. T. Komm, S. Strobel, T. Schleid, Two potassium gadolinium(III) ortho-thiophosphates(V): K<sub>3</sub>Gd<sub>3</sub>[PS<sub>4</sub>]<sub>4</sub> and K<sub>9</sub>Gd[PS<sub>4</sub>]<sub>4</sub>. *J Alloys Compd.* 2008;451(1-2):648-653. doi:10.1016/j.jallcom.2007.04.080
12. V.V. Klepov, K.A. Pace, L.S. Breton, V. Kocevski, T.M. Besmann, H.C. zur Loye, Nearly Identical but Not Isotypic: Influence of Lanthanide Contraction on Cs<sub>2</sub>NaLn(PS<sub>4</sub>)<sub>2</sub> (Ln=La–Nd, Sm, and Gd–Ho). *Inorg Chem.* 2020;59(3):1905–1916. doi:10.1021/acs.inorgchem.9b03200

13. T. Schleid, I. Hartenbach, T. Komm,  $K_2NdP_2S_7$ : A Mixed Valent Neodymium(III) Thiophosphate According to  $K_4Nd_2[PS_4]_2[P_2S_6]$  with Discrete  $[PS_4]^{3-}$  and  $[S_3P-PS_3]^{4-}$  Anions. *Z Anorg Allg Chem.* 2002;628:7-9.
14. E.Y. Goh, E.J. Kim, S.J. Kim. Structure modification on quaternary rare earth thiophosphates:  $NaYbP_2S_6$ ,  $NaSmP_2S_6$ , and  $KSmP_2S_7$ . *J Solid State Chem.* 2001;160(1):195-204. doi:10.1006/jssc.2001.9222
15. R.F. Hess, P.L. Gordon, C.D. Tait, K.D. Abney, P.K. Dorhout. Synthesis and structural characterization of the first quaternary plutonium thiophosphates:  $K_3Pu(PS_4)_2$  and  $APuP_2S_7$  (A = K, Rb, Cs). *J Am Chem Soc.* 2002;124(7):1327-1333. doi:10.1021/ja0108133
16. A. Kuhn, R. Eger, J. Nuss, B.V. Lotsch. Synthesis and structural characterization of the alkali thiophosphates  $Na_2P_2S_6$ ,  $Na_4P_2S_6$ ,  $K_4P_2S_6$ , and  $Rb_4P_2S_6$ . *Zeitschrift fur Anorg und Allg Chemie.* 2014;640(5):689-692. doi:10.1002/zaac.201300575
17. C.R. Evenson IV, P.K. Dorhout. Thiophosphate phase diagrams developed in conjunction with the synthesis of the new compounds  $KLaP_2S_6$ ,  $K_2La(P_2S_6)_{1/2}(PS_4)$ ,  $K_3La(PS_4)_2$ ,  $K_4La_{0.67}(PS_4)_2$ ,  $K_{9-x}La_{1+x/3}(PS_4)_4$  (x = 0.5). *Inorg Chem.* 2001;40(12):2884-2891. doi:10.1021/ic000596r
18. L.M. Schoop, R. Eger, R.K. Kremer, A. Kuhn, J. Nuss, B.V. Lotsch. Structural Stability Diagram of  $ALnP_2S_6$  Compounds (A = Na, K, Rb, Cs; Ln = Lanthanide). *Inorg Chem.* 2017;56(3):1121-1131. doi:10.1021/acs.inorgchem.6b02052
19. L.M. Schoop, R. Eger, J. Nuss, F. Pielhofer, B.V. Lotsch. The First Quinary Rare Earth Thiophosphates:  $Cs_5Ln_3X_3(P_2S_6)_2(PS_4)$  (Ln = La, Ce, X = Br, Cl) and the Quasi-Quaternary  $Cs_{10}Y_4Cl_{10}(P_2S_6)_3$ . *Zeitschrift fur Anorg und Allg Chemie.* 2017;643(23):1818-1823. doi:10.1002/zaac.201700309
20. T. Komm, T. Schleid. The first rubidium rare-earth(III) thiophosphates:  $Rb_3M_3[PS_4]_4$  (M=Pr, Er). *J Solid State Chem.* 2005;178(2 SPEC. ISS.):454-463. doi:10.1016/j.jssc.2004.07.048
21. A. Mesbah, J. Prakash, J.C. Beard, S. Lebègue, C.D. Malliakas, J.A. Ibers. Syntheses, crystal structures, optical and theoretical studies of the actinide thiophosphates  $SrU(PS_4)_2$ ,  $BaU(PS_4)_2$ , and  $SrTh(PS_4)_2$ . *Inorg Chem.* 2015;54(6):2970-2975. doi:10.1021/acs.inorgchem.5b00071
22. V.V Klepov, C.A. Juillerat, K.A. Pace, G. Morrison, H.C. zur Loye. "Soft" Alkali Bromide and Iodide Fluxes for Crystal Growth. *Front Chem.* 2020;8(June):1-18. doi:10.3389/fchem.2020.00518
23. H.C. zur Loye, T. Besmann, J. Amoroso, et al. Hierarchical Materials as Tailored Nuclear Waste Forms: A Perspective. *Chem Mater.* 2018;30(14):4475-4488. doi:10.1021/acs.chemmater.8b00766
24. G. Gauthier, S. Jobic, R. Brec, J. Rouxel.  $K_3CeP_2S_8$ : A New Cerium Thiophosphate with One-Dimensional Anionic Chains. *Inorg Chem.* 1998;37:2332-2333.

doi:10.1021/ic980091p

25. M. Ohta, S. Hirai, H. Kato, V.V. Sokolov., V.V. Bakovets. Thermal decomposition of  $\text{NH}_4\text{SCN}$  for preparation of  $\text{Ln}_2\text{S}_3$  (Ln=La and Gd) by sulfurization. *Mater Trans.* 2009;50(7):1885-1889. doi:10.2320/matertrans.M2009060
26. SAINT; Bruker AXS Inc.: Madison, WI, 2012. 2012.
27. L. Krause, R. Herbst-Irmer, G.M. Sheldrick, D. Stalke. Comparison of silver and molybdenum microfocus X-ray sources for single-crystal structure determination. *J Appl Crystallogr.* 2015;48(1):3-10. doi:10.1107/S1600576714022985
28. O.V. Dolomanov, L.J. Bourhis, R.J. Gildea, J.A.K. Howard, H. Puschmann. OLEX2: A complete structure solution, refinement and analysis program. *J Appl Crystallogr.* 2009;42(2):339-341. doi:10.1107/S0021889808042726
29. G.M. Sheldrick. Crystal structure refinement with SHELXL. *Acta Crystallogr Sect C Struct Chem.* 2015;71(Md):3-8. doi:10.1107/S2053229614024218
30. G. Morrison, H.C. zur Loye. Simple correction for the sample shape and radial offset effects on SQUID magnetometers: Magnetic measurements on  $\text{Ln}_2\text{O}_3$  (Ln=Gd, Dy, Er) standards. *J Solid State Chem.* 2015;221:334-337. doi:10.1016/j.jssc.2014.10.026
31. S. Seidlmayer. Strukturchemische Untersuchungen an Hexachalkogenohypodiphosphaten und verwandten Verbindungen. 2010. <https://pub.uni-regensburg.de/13427/>.
32. M.A. McGuire, T.K. Reynolds, F.J. DiSalvo. Exploring thallium compounds as thermoelectric materials: Seventeen new thallium chalcogenides. *Chem Mater.* 2005;17(11):2875-2884. doi:10.1021/cm050412c
33. K. Binnemans, C. Görller-Walrand. On the color of the trivalent lanthanide ions. *Chem Phys Lett.* 1995;235(3-4):163-174. doi:10.1016/0009-2614(95)00126-O
34. S.K. Malik, R. Vijayaraghavan. Crystal field effects on the saturation magnetic moment of  $\text{Sm}^{3+}$  ion in ferromagnetic samarium compounds. *Pramana.* 1974;3(2):122-132.
35. N.N. Greenwood, A. Earnshaw. *Chemistry of the Elements.* 2nd Editio. Oxford; 1997.